Spin-dependent neutralino-nucleus scattering for $A \sim 127$ nuclei

M. T. Ressell
W.K. Kellogg Radiation Laboratory, 106-38, California Institute of Technology, Pasadena, California 91125

D. J. Dean
Physics Division, Oak Ridge National Laboratory, Oak Ridge, Tennessee 37831

(Received 10 February 1997)

We perform nuclear shell model calculations of the neutralino-nucleus cross section for several nuclei in the $A=127$ region. Each of the four nuclei considered is a primary target in a direct dark matter detection experiment. The calculations are valid for all relevant values of the momentum transfer. Our calculations are performed in the $3s2d1g_{7/2}1h_{11/2}$ model space using extremely large bases, allowing us to include all relevant correlations. We also study the dependence of the nuclear response upon the assumed nuclear Hamiltonian and find it to be small. We find good agreement with the observed magnetic moment as well as other obervables for the four nuclei considered: ^{127}I, ^{129,131}Xe, and ^{125}Te. [S0556-2813(97)00707-3]

PACS number(s): 95.35.+d, 95.30.Cq, 14.80.Ly, 21.60.Cs

I. INTRODUCTION

An ever increasing amount of evidence indicates the existence of large amounts of dark matter in the Universe [1]. Despite this overwhelming evidence, the exact nature of the dark matter remains a mystery. Numerous candidates have been proposed, including both baryonic and nonbaryonic matter [2]. Observations reveal that some of the dark matter in the Galactic halo is baryonic, consisting of massive compact halo objects (MACHO's) [3]; however, present data indicates that MACHO's cannot account for all of the dark matter implied by the Galactic rotation curve [4]. Furthermore, a number of arguments based upon large scale motions in the Universe and large scale structure formation indicate that $\Omega \approx 1$, which is far in excess of the bounds on $\Omega_{\rm baryon} h^2 \leq 0.026$ arising from cosmic nucleosynthesis [5]. All considerations point toward nonbaryonic matter comprising a sizable fraction of the Universal density. If this is true, what is the dark matter?

Among the best motivated, and hence highly favored, of the nonbaryonic dark matter candidates is the lightest supersymmetric particle (LSP). Experimental and theoretical considerations indicate that the LSP is a neutralino, $\widetilde{\chi}$, consisting of a linear combination of the supersymmetric partners of the photon ($\widetilde{\gamma}$), the Z ($\widetilde{Z}$), and two Higgs bosons ($\widetilde{H}_1$ and $\widetilde{H}_2$). Note that the $\widetilde{\gamma}$ and $\widetilde{Z}$ are themselves linear combinations of the supersymmetric partners of the neutral W ($\widetilde{W}_3$) and B ($\widetilde{B}$) bosons, hence the neutralino composition is typically written as

$$\widetilde{\chi} = Z_1 \widetilde{B} + Z_2 \widetilde{W}_3 + Z_3 \widetilde{H}_1 + Z_4 \widetilde{H}_2 . \quad (1)$$

The motivation for supersymmetry (SUSY) arises naturally in modern theories of particle physics [1,6], although the $\widetilde{\chi}$'s potential as a dark matter candidate was not realized until later [7]. For a very large region of SUSY parameter space, neutralinos provide densities that are in accord with the measured value of Ω, thus explaining the dark matter. The $\widetilde{\chi}$ is also detectable in at least two ways: indirectly, through the products of $\widetilde{\chi}\widetilde{\chi}$ annihilation in the Sun, Earth, and Galactic halo [1,8], or directly, via elastic (and inelastic [9]) neutralino-nucleus ($\widetilde{\chi}N$) scattering in a detector [1,10]. In either case, the elastic $\widetilde{\chi}N$ scattering cross section is an essential ingredient. In this paper we discuss nuclear structure calculations relevant to $\widetilde{\chi}N$ scattering for several nuclei which are primary constituents of many current and planned direct detection experiments [9,11–15].

Physics at three distinct energy scales governs $\widetilde{\chi}N$ scattering. The composition and mass of the $\widetilde{\chi}$, and hence its interaction with quarks, are fixed near the electroweak scale. The interaction of neutralinos with protons and neutrons is determined by the quark distribution (both spin and density) within the nucleon, which is determined at the QCD scale. At the modest momentum transfers available to dark matter neutralinos the $\widetilde{\chi}$ interacts with the entire nucleus, not individual nucleons within it. Thus, nuclear structure plays an important role in determining the $\widetilde{\chi}N$ cross section. The uncertainties in the electroweak scale physics (the SUSY part of the problem) are typically handled by considering large sweeps through SUSY parameter space [1,11,16]. The QCD scale physics is currently the focus of much study and the relevant nucleon matrix elements continue to be measured with high precision [17]. The necessary nuclear physics is not measurable for most nuclei but is amenable to calculation through a variety of methods. Here we apply the nuclear shell model to the nuclei ^{127}I, ^{129}Xe, ^{131}Xe, ^{125}Te, and ^{23}Na (this last nucleus we discuss in an appendix) in order to provide a consistent and correct set of nuclear input physics for determining the $\widetilde{\chi}N$ cross section.

The $\widetilde{\chi}N$ scattering cross section has two distinct terms: a spin-independent, or *scalar*, term, and a spin-dependent, or *axial*, term. It has been well established that for nuclei with $A > 30$–50 ($A \equiv$ number of nucleons), the scalar piece of the interaction tends to dominate the $\widetilde{\chi}N$ scattering rate; however, there are significant regions of parameter space where this is not so and the axial rate dominates [1,16]. The importance of understanding the axial $\widetilde{\chi}N$ interaction is amply

demonstrated by a recent SUSY interpretation of a Fermilab scattering event [18]. These papers claim that the $\widetilde{\chi}$ might be an almost pure Higgsino whose couplings to ordinary matter are completely dominated by the axial part. In this paper, we shall deal with the axial $\widetilde{\chi}N$ interaction. The relevant nuclear physics for the scalar interaction is well approximated by a fairly simple form factor, suitable for all nuclei [19,20]. The axial response is far more complicated and requires detailed nuclear models.

II. NUCLEAR PHYSICS INPUT

A variety of nuclear models have been used to calculate the axial response of nuclei used as targets in dark matter detectors. The conventional nuclear shell model [21] has proven highly successful at accurately representing this response when a reasonable nuclear Hamiltonian is used in a sufficiently large model space [22–25]. Until recently, both of these ingredients have been absent for nuclei in the $3s2d1g_{7/2}1h_{11/2}$ shell, including most of those included in this study. With recent advances in computer power and storage, we can now construct model spaces that contain most of the nuclear configurations that are likely to dominate the spin response of nuclei such as ^{127}I. Coupled with this ability to perform sufficiently large calculations is the recent development of several realistic nucleon-nucleon (nn) potentials [26,27]. These potentials can then be converted into suitable nuclear interaction Hamiltonians via the G-matrix–folded diagram technique [26]. In this paper we consider two such nuclear interactions, one using the Bonn A [26] and the other the Nijmegen II [27] nn potential. The diagonalization of the Hamiltonian was performed using the shell model code ANTOINE [28].

A. The Hamiltonian

The residual nuclear interaction based upon the Bonn A potential has been described in Ref. [26]. This Hamiltonian has been derived for the model space consisting of the $1g_{7/2}$, $2d_{5/2}$, $3s_{1/2}$, $2d_{3/2}$, and $1h_{11/2}$ orbitals (which we use in this study). It was originally derived to describe light Sn isotopes ($A\approx 102$–110) which have no protons in the space. In order to find good agreement with observables for nuclei with $A\approx 130$, the single-particle energies (SPE's) were adjusted. We made an initial guess at the SPE's based upon the excited state energy spectra of nuclei with either a single-neutron hole in the space (^{131}Sn) or a single proton in the space (^{133}Sb and ^{125}Sb). These initial SPE's were then used in conjunction with the two-body matrix elements (TBME's) of the interaction to calculate observables for the nucleus ^{127}I. We varied the SPE's until reasonable agreement between calculation and experiment was found for the following ^{127}I observables: the magnetic moment (μ), the low lying excited state energy spectrum, and the quadrupole moment (Q_{20}). This procedure is similar to that performed in Ref. [22]. The magnetic moment is extremely important, as it is the observable most closely related to the $\widetilde{\chi}N$ scattering matrix element and has traditionally been used as a benchmark of a calculation's accuracy. In Fig. 1, we show the final SPE's used in our calculations. In Table I we show the final calculated values of μ and Q_{20} for ^{127}I vs the experimental values; agreement is excellent. Once the SPE's are specified, we have a reasonable Hamiltonian to use for the nuclei we are studying.

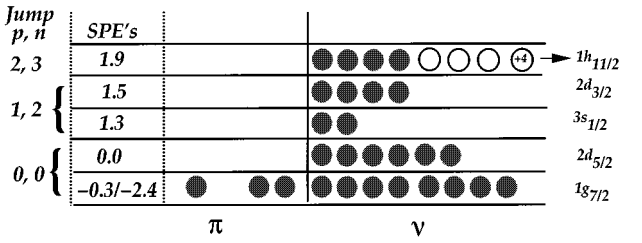

FIG. 1. A visual description of the ^{127}I model space. See the text for specific details of the construction of the space. The other nuclei studied use the same jump assignments and SPE's. The left $1g_{7/2}$ SPE is that used for the Bonn A interaction and the one on the right is used by the Nijmegen II interaction.

In order to test the sensitivity of our results to the nuclear Hamiltonian, we have also examined another one, derived from the Nijmegen II nn potential [27]. We have used the codes and methods described in [29] to convert the potential to a usable shell model interaction. The procedure is similar to that used for the Bonn A force. The two sets of TBME's are generally similar but significant differences do exist. We initially used the same set of SPE's as above but found that a significant lowering of the $1g_{7/2}$ SPE was necessary in order to find agreement with the observables. The SPE's and comparisons with observables for this force are shown in Fig. 1 and Tables I and II.

B. The model space

To perform a full basis, positive parity, calculation of the ^{127}I ground state properties in the space consisting of the $1g_{7/2}$, $2d_{5/2}$, $3s_{1/2}$, $2d_{3/2}$, and $1h_{11/2}$ orbitals, we would need to have basis states consisting of roughly 1.3×10^9 Slater determinants (SD's). Current, state of the art, calculations (including those presented here) can diagonalize matrices with basis dimensions in the range 1–2×10^7 SD's; clearly severe truncations of the model space are needed. Fortunately, given the size of the model spaces that can be treated, a truncation scheme that includes the majority of relevant configurations can be devised.

Our scheme is best understood by viewing Fig. 1. As a base configuration, we have for protons $(1g_{7/2}2d_{5/2})^3$ (i.e., a total of three protons spread among the $1g_{7/2}$ and $2d_{5/2}$ orbitals) and for neutrons $(1g_{7/2}2d_{5/2})^{14}+(3s_{1/2}2d_{3/2})^6+(1h_{11/2})^4$. We then assign the following values of the

TABLE I. The calculated magnetic and quadrupole moments of ^{127}I compared to experiment for calculations using both effective interactions. For the quadrupole moment, effective charges of $e_p=1.5e$ and $e_n=0.5e$ have been used. The magnetic moment calculations use the free particle g factors. We also include the ISPSM estimates of the quantities in order to illustrate the quenching obtained.

Observable	ISPSM	Bonn A	Nijmegen II	Experiment
μ	4.79	2.775	3.150	2.813
Q_{20}	−0.654	−0.577	−0.577	−0.789

TABLE II. A comparison of various calculations of the spin distribution of ^{127}I, ^{129}Xe, ^{131}Xe, and ^{125}Te. Bonn A and Nijmegen II are the calculations presented here. OGM is the odd group model of [30]. IBFM is the interacting boson Fermion model of [31]. TFFS is the theory of finite Fermi systems calculation of [33]. QTDA is the quasi Tamm-Dancoff approximation of [20]. A blank entry means that the value of that particular angular momentum component was not presented in the reference. An entry of N/A in the magnetic moment column implies that the experimental magnetic moment was used to find the values of spin $\langle \mathbf{S}_p \rangle$ or $\langle \mathbf{S}_n \rangle$ shown. Calculations of the magnetic moment using effective g factors as described in the text are given in parenthesis.

	$\langle \mathbf{S}_p \rangle$	$\langle \mathbf{S}_n \rangle$	$\langle \mathbf{L}_p \rangle$	$\langle \mathbf{L}_n \rangle$	μ
^{127}I					
Experiment					2.813
Bonn A	0.309	0.075	1.338	0.779	2.775 (2.470)
Nijmegen II	0.354	0.064	1.418	0.664	3.150 (2.790)
OGM [30]	0.07	0.0	2.43	0.0	N/A
IBFM [31]	0.154	0.0034			N/A
TFFS [33]	0.15				
ISPSM [32]	0.5	0.0	2.0	0.0	4.793
^{129}Xe					
Experiment					−0.778
Bonn A	0.028	0.359	0.227	−0.114	−0.983 (−0.634)
Nijmegen II	0.0128	0.300	0.372	−0.185	−0.701 (−0.379)
OGM [30]	0.0	0.2	0.0	0.3	N/A
IBFM [31]	0.0	0.2			N/A
TFFS [33]		0.25			
ISPSM [32]	0.0	0.5	0.0	0.0	−1.913
^{131}Xe					
Experiment					0.69
Bonn A	−0.009	−0.227	0.165	1.572	0.980 (0.637)
Nijmegen II	−0.012	−0.217	0.215	1.514	0.979 (0.347)
QTDA [20]	−0.041	−0.236	0.026	1.751	0.70
OGM [30]	0.0	−0.18	0.0	1.68	N/A
IBFM [31]	0.0	−0.17			N/A
TFFS [33]		−0.186			
ISPSM [32]	0.0	−0.3	0.0	1.8	1.71
^{125}Te					
Experiment					−0.889
Bonn A	0.001	0.287	0.077	0.135	−1.015 (−0.749)
Nijmegen II	−0.0003	0.323	0.102	0.075	−1.134 (−0.824)
OGM [30]	0.0	0.23	0.0	0.27	N/A
IBFM [31]	−0.0004	0.23			N/A
TFFS [33]		0.22			
ISPSM [32]	0.0	0.5	0.0	0.0	−1.913

''jump'' to each proton {neutron} orbital: jump($1g_{7/2}$,$2d_{5/2}$) = 0 {0}, jump($3s_{1/2}$,$2d_{3/2}$) = 1 {2}, and jump($1h_{11/2}$) = 2{3}. The differences in these values is the cost of moving particles between the different (sets of) orbitals. Hence, to move a proton {neutron} from the $1g_{7/2}$ to the $2d_{5/2}$ costs nothing while moving one from the $1g_{7/2}$ to the $3s_{1/2}$ would cost 1 {2} unit{s} of jump (to the $1h_{11/2}$ would cost 2 {3} units). It would cost 2 units of jump to move 2 neutrons from the $2d_{3/2}$ to the $1h_{11/2}$, etc. All that remains is to specify the total amount of jump available. In our truncation, we allow protons up to 3 units of jump, neutrons up to 4 units, and a total of up to 4 when adding the jump used by the protons plus neutrons. Thus, if the protons remain in the $1g_{7/2}$ and $2d_{5/2}$ orbitals (as they tend to do), the following neutron configurations are allowed: $(1g_{7/2}2d_{5/2})^{14}+(3s_{1/2}2d_{3/2})^{6}+(1h_{11/2})^{4}$, $(1g_{7/2}2d_{5/2})^{14}+(3s_{1/2}2d_{3/2})^{4}+(1h_{11/2})^{6}$, $(1g_{7/2}2d_{5/2})^{13}+(3s_{1/2}2d_{3/2})^{5}+(1h_{11/2})^{6}$, and $(1g_{7/2}2d_{5/2})^{14}+(3s_{1/2}2d_{3/2})^{2}+(1h_{11/2})^{8}$. If 1 or 2 protons are excited out of the $1g_{7/2}$ and $2d_{5/2}$ orbitals, the last two neutron configurations are not allowed. In this truncation, the m-scheme dimension of the ^{127}I model space is about 3 million SD's.

TABLE III. The proton (p) and neutron (n) occupation numbers obtained for each orbital in the ^{127}I calculations. The points to notice are the similarities between the two different interactions and the fact that the $1h_{11/2}n$ number is significantly less than 8, the maximum number allowed.

Orbital	Bonn A	Nijmegen II
$1g_{7/2}p$	1.97979	1.83023
$1g_{7/2}n$	7.87440	7.94902
$2d_{5/2}p$	0.89648	0.95545
$2d_{5/2}n$	5.92205	5.93768
$3s_{1/2}p$	0.02859	0.09023
$3s_{1/2}n$	1.57985	1.71861
$2d_{3/2}p$	0.09511	0.12374
$2d_{3/2}n$	2.62799	2.71644
$1h_{11/2}p$	0.00004	0.00034
$1h_{11/2}n$	5.99571	5.67825

Our results indicate that this space is more than adequate to describe the ground state properties of the nuclei considered. As mentioned above, our calculation of the observables agrees well with experiment. The major potential problem with this model space would be if it failed to allow enough neutron excitations into the $1h_{11/2}$ orbital. It allows at most 8 neutrons out of a possible 12 in that orbital. In Table III we present the occupation numbers for ^{127}I. We see that our interactions do not seem to prefer excitation of more than one extra neutron pair to the $1h_{11/2}$. Most configurations have six neutrons in that orbital, while eight are allowed. Hence, our model space is more than adequate.

For the two xenon isotopes considered ($A=129$ and 131), we have used exactly this truncation scheme. For ^{125}Te we used this scheme and also one where the total jump and total neutron jump was 6 (instead of 4). Very little difference was noticed for the two truncations. In this paper we present the results for the larger truncation since it should be slightly more realistic.

III. RESULTS

A. The zero-momentum transfer limit

Neutralinos in the halo of our Galaxy are characterized by a mean virial velocity of $v \simeq \langle v \rangle \simeq 300$ km/sec$=10^{-3}c$. The maximum characteristic momentum transfer in $\tilde{\chi}N$ scattering is $q_{\max}=2M_r v$ where M_r is the reduced mass of the

$\tilde{\chi}N$ system. If the product $q_{\max}R$ is small ($\ll 1$), where R is the nuclear size, the matrix element for spin-dependent $\tilde{\chi}N$ scattering reduces to a very simple form [1,19]

$$\mathcal{M}=C\langle N|a_p\mathbf{S}_p+a_n\mathbf{S}_n|N\rangle\cdot\mathbf{s}_{\tilde{\chi}}, \tag{2}$$

where

$$\mathbf{S}_i=\sum_k \mathbf{s}_i(\mathbf{k}), \quad i=p,n \tag{3}$$

is the total nuclear spin operator, k is a sum over all nucleons, and a_p, a_n are $\tilde{\chi}$-nucleon coupling constants which depend upon the quark spin distribution within the nucleons and on the composition of the $\tilde{\chi}$. In keeping with previous work [19,22] we use the convention that all angular momentum operators are evaluated in their z projection in the maximal M_J state, e.g., $\langle\mathbf{S}\rangle\equiv\langle N|\mathbf{S}|N\rangle=\langle J,M_J=J|S_z|J,M_J=J\rangle$. Much of the uncertainties arising from electroweak and QCD scale physics are encompassed by a_p and a_n. The normalization C involves the coupling constants, masses of the exchanged bosons, and various LSP mixing parameters that have no effect upon the nuclear matrix element. Equation (2) has often been written as

$$\mathcal{M}=C\Lambda\langle N|\mathbf{J}|N\rangle\cdot\mathbf{s}_{\tilde{\chi}} \tag{4}$$

with

$$\Lambda=\frac{\langle N|a_p\mathbf{S}_p+a_n\mathbf{S}_n|N\rangle}{\langle N|\mathbf{J}|N\rangle}=\frac{\langle N|(a_p\mathbf{S}_p+a_n\mathbf{S}_n)\cdot\mathbf{J}|N\rangle}{J(J+1)}. \tag{5}$$

Examples of the full $\tilde{\chi}N$ cross section can be found in Refs. [1,19,22].

Equations (2)–(5) show that the $\tilde{\chi}$ couples to the spin carried by the protons and the neutrons. The matrix element (2) is similar to the magnetic moment operator:

$$\mu=\langle N|g_n^s\mathbf{S}_n+g_n^l\mathbf{L}_n+g_p^s\mathbf{S}_p+g_p^l\mathbf{L}_p|N\rangle. \tag{6}$$

The *free particle* g factors are given by $g_n^s=-3.826$, $g_n^l=0$, $g_p^s=5.586$, and $g_p^l=1$ (in nuclear magnetons). Given the similarities of Eqs. (2) and (6), it is no surprise that μ is often used as a benchmark on the accuracy of the calculation of $\mathbf{S}_p$and $\mathbf{S}_n$ in Λ. We follow that prescription as well. In the following section we will briefly outline some problems with this procedure.

In Table II we present the values for $\mathbf{S}_p$, $\mathbf{S}_n$, $\mathbf{L}_p$, $\mathbf{L}_n$, and μ that we calculate for each Hamiltonian for the nuclei ^{127}I, ^{129}Xe, ^{131}Xe, and ^{125}Te. We also include the experimentally measured magnetic moment, it is apparent that agreement is quite good for all nuclei. A number of other calculations of these quantities appear in the literature, and we include summaries of these calculations in the table as well. The following abbreviations are used for the various nuclear models: Bonn A, our calculation using the Bonn A derived force; Nijmegen II, our calculation using the Nijmegen II derived force; OGM, the odd group model [30]; IBFM, the interacting boson fermion model [31]; ISPSM, the independent single particle shell model [32]; TFFS, the theory of finite Fermi systems [33]; and QTDA, the quasi Tamm-Dancoff approximation [20]. In most previous experimental analyses, the OGM values have been used [12,13].

Examining our results for $\mathbf{S}_p$and $\mathbf{S}_n$ in Table II and comparing them to results from other nuclear models reveal several interesting facts. In almost every instance, our results show that the spin $|\mathbf{S}_i|$ $(i=p,n)$ carried by the unpaired nucleon is greater than that found in the other nuclear models (except for the ISPSM, where $|\mathbf{S}_i|$ is maximal). Despite our larger values for $|\mathbf{S}_i|$, our calculations have significant quenching of the magnetic moment and are in good agreement with experiment in all cases (see the later section on quenching). The reason that we find larger values of $|\mathbf{S}_i|$ for the odd group is due to the fact that we allow more excitation of the even group of the nuclei, allowing them to be a major contributor to the total nuclear spin: $\mathbf{J}=\mathbf{S}_p+\mathbf{S}_n+\mathbf{L}_p+\mathbf{L}_n$. The naive expectation for $\mathbf{L}_n$ in the Bonn A calculation of ^{127}I is zero. We find $\mathbf{L}_n=0.779$, $\mathbf{L}_n$ is responsible for over 30% of iodine's total angular momentum ($\mathbf{J}=\frac{5}{2}$). This explains both the large quenching of μ ($\mathbf{L}_n$ does not contribute to μ since $g_n^l=0$) and the large value of $\mathbf{S}_p$ found. We note that most previous experimental analyses used the OGM value for ^{127}I, $\mathbf{S}_p=0.07$. Our results give a factor of ~ 20 increase in iodine's sensitivity to spin-dependent scattering over that previously assumed. Due to the form factor suppression (discussed below) a sodium iodide detector's [11,13] spin response is still dominated by ^{23}Na but not to the extent previously thought. For the remainder of the nuclei considered, Table II also reveals increased scattering sensitivity, although the factor of increase is much more modest.

B. Quenching and uncertainties

As we noted earlier, the comparison of the computed magnetic moment vs the experimental value has been used as the primary (and in some cases, only) indicator of a calculation's reliability. This seems quite reasonable in light of the similarities between the matrix elements in Eqs. (2) and (6). This prescription is not without several potential problems [22,34]. Not only does μ depend upon the orbital angular momentum $\mathbf{L}_i$ but the spin angular momentum $\mathbf{S}_i$ is subtly different. The $\tilde{\chi}N$ matrix element (2) results from the nonrelativistic reduction of the axial-vector current. Because of this, it is not strongly affected by meson exchange currents (MEC's). The magnetic moment's spin operators, $\mathbf{S}_i$, are a result of the nonrelativistic reduction of the vector current. They can be strongly affected by MEC's [23,34]. The effects of MEC's upon μ is typically lumped together with several other effects to give effective g factors [35,36]. Unfortunately, there is no hard and fast rule as to what effective g factors are the best. We have chosen to remain with the free particle g factors. As an example of the potential uncertainties this ambiguity leads to, we have also included, in Table II, the calculated magnetic moment for our nuclei using a reasonable set of effective g factors. The ''quenched'' magnetic moments are the values in parentheses in the table and the effective g factors used are: $g_n^s=-2.87$, $g_n^l=-0.1$, $g_p^s=4.18$, and $g_p^l=1.1$. The table shows that these g factors do little, overall, to improve the concordance between calculation and experiment.

A related concern involves the quenching of the (isovector) Gamow-Teller (GT) g factor, g_A [22,34]. The spin term of the GT operator also comes from the axial-vector current and thus is closely related to the spin operators in Eq. (6). Its is well established that most nuclear model calculations of GT strength require a reduction of g_A of order 20% [21]. Whether this quenching of g_A should also be applied to a_1 (the isovector $\tilde{\chi}$-nucleon coupling constant) is unknown [34]. Since there is no real guidance, and our magnetic moments agree well with experiment, we do not believe that any extra quenching of the spin matrix elements (or equivalently the coupling constants a_0 and a_1) is desirable for these nuclei when calculating $\tilde{\chi}N$ scattering rates. Nonetheless, as pointed out in Ref. [34], it is useful to keep these potential uncertainties in mind when calculating scattering rates.

C. Finite momentum transfer

When the LSP was first proposed as a viable dark matter candidate, its preferred mass was between 5 and 10 GeV [7]. With a mass of this order and a typical galactic halo velocity ($v \simeq 10^{-3}c$), the neutralino's total momentum ($q \sim M_r v \sim 10$ MeV) was small compared to the inverse of the nuclear size ($1/R \sim 1/1$ fm ~ 200 MeV) and the zero-momentum transfer limit was appropriate for studies of $\tilde{\chi}N$ scattering. Since then, experiments at accelerators have pushed the allowed $\tilde{\chi}$ mass, $m_{\tilde{\chi}}$, to larger values (there are ways around this if some of the theoretical assumptions are relaxed [37]), and it has been shown that heavy $\tilde{\chi}$'s are just as viable as a dark matter candidate as the lighter ones [38,39]. As $m_{\tilde{\chi}}$ becomes larger than a few 10's of GeV the product qR starts to become non-negligible and finite momentum transfer must be considered for heavier nuclei.

The formalism for elastic $\tilde{\chi}N$ scattering at all momentum transfers has been developed in Refs. [19,20]. Here, we follow precisely the definitions used in [22]. It is a simple matter to go from our definitions to those used in Ref. [1]. The formalism is a straightforward extension of that developed for the study of weak and electromagnetic semileptonic interactions in nuclei [40]. The differential $\tilde{\chi}N$ cross section is given by

$$\frac{d\sigma}{dq^2} = \frac{8G_F^2}{(2J+1)v^2} S(q), \tag{7}$$

where $S(q)$ is the spin structure function

$$S(q) = \sum_{L\ \mathrm{odd}} \left(|\langle N \| \mathcal{T}^{\mathrm{el5}}_L(q) \| N \rangle|^2 + |\langle N \| \mathcal{L}^5_L(q) \| N \rangle|^2 \right). \tag{8}$$

$\mathcal{T}^{\mathrm{el5}}(q)$ and $\mathcal{L}^5(q)$ are the transverse electric and longitudinal multipole projections of the axial-vector current operator [40]. The double vertical lines imply that these are the reduced matrix elements of these operators. For their explicit form in the $\tilde{\chi}$ context, see [19,20,22]. In the limit of zero-momentum transfer $S(q)$ reduces to

$$S(0) = \frac{2J+1}{\pi} \Lambda^2 J(J+1). \tag{9}$$

The reduced matrix elements of the multipoles in Eq. (8) are easily evaluated in the harmonic oscillator basis in the nuclear shell model [40]. With the exception of the calculation of the ^{27}Al structure function in [23] all calculations of $S(q)$ have used bases of these harmonic oscillator wave functions. In this paper, we have used the more realistic Woods-Saxon wave functions to evaluate Eq. (8). To specify the wave functions, we use the parameters recommended in [41]. We have used the codes from [42] to calculate the actual wave functions. We have also calculated the Bonn A structure function for ^{127}I using harmonic oscillator wave functions. The differences in the two prescriptions are significant at very large momentum transfers but are minor at most relevant values of of the momentum transfer (q).

It is useful (and traditional) to use the isospin convention instead of the proton-neutron formalism when discussing $\tilde{\chi}N$ scattering at finite momentum transfer. Writing the isoscalar coupling constant as $a_0 = a_n + a_p$ and the corresponding isovector coupling constant as $a_1 = a_p - a_n$ we may split $S(q)$ into a pure isoscalar term, S_{00}, a pure isovector term, S_{11}, and an interference term, S_{01}, in the following way:

$$S(q) = a_0^2 S_{00}(q) + a_1^2 S_{11}(q) + a_0 a_1 S_{01}(q). \tag{10}$$

Using this decomposition of $S(q)$ it is a simple matter to derive the structure function for a $\tilde{\chi}$ of arbitrary composition.

Two factors contribute to the maximum allowed momentum transfer. As $m_{\tilde{\chi}}$ becomes much greater than the nuclear mass, m_N, the reduced mass asymptotes to $M_r \to m_N$. Also, the $\tilde{\chi}$'s have a Maxwellian velocity distribution in the halo and some will possess velocities significantly greater than $\langle v \rangle \simeq 10^{-3}c$. A maximum velocity of $v_{\max} \simeq 700$ km/sec (slightly greater than Galactic escape velocity [14]) implies maximum momentum transfers of $q_{\max}(A \sim 127) \simeq 550$ MeV. This value is not *small* compared to the inverse nuclear size. In a harmonic oscillator basis, the fiducial nuclear size is set by the oscillator parameter, $b = 1\ \mathrm{fm}\ A^{1/6} = (1/197.327\ \mathrm{MeV}) A^{1/6}$. In order to maintain contact with previous literature [22,23] we retain b as the size parameter in our Woods-Saxon evaluations of $S(q)$. We do, however, use a slightly better, empirical, parametrization of b [43]: $b = (41.467/\hbar\omega)^{1/2}$ fm with $\hbar\omega = 45A^{-1/3} - 25A^{-2/3}$ MeV. Hence, we have values near $b(A=127) = 2.282$ fm $= 1/86.47$ MeV for the nuclei in this study. We parametrize all of our structure functions in terms of $y \equiv (qb/2)^2$. For $y \ll 1$ the effects of finite momentum transfers are small; for $y \geq 1$ the effects are quite noticeable. For these nuclei $y_{\max} = (q_{\max} b/2)^2 \simeq 10 \gg 1$, hence nuclear form factors are extremely significant. These extremely large values of y are only valid for extremely massive $\tilde{\chi}$'s moving near escape velocity. A more realistic $\tilde{\chi}$, with $m_{\tilde{\chi}} = 100$ GeV moving at $\langle v \rangle$ would have $y_{\max} \simeq 0.4$.

In order to cover all of the relevant $\tilde{\chi}$ parameter space, we have evaluated the structure functions all the way to $y = 10$ for the nuclei studied. This presents a problem in that it has become standard to present structure functions as polynomials in y of order 6 or less. (A structure function of this sort can easily be incorporated into the code NEUTDRIVER of Ref. [1].) We could find no suitable fits of this form valid out

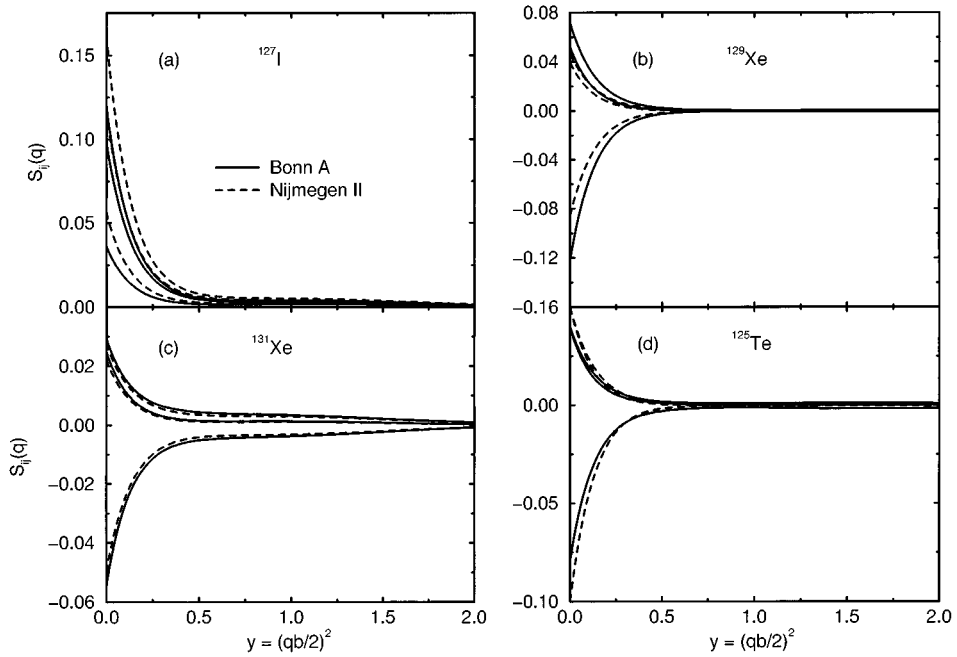

FIG. 2. The three spin structure functions $S_{ij}(q)$ where $i,j=0,1$ for the four nuclei considered. The results using both effective interactions are plotted. Accurate fits to these structure functions can be found in Appendices B and C. (a) $S_{ij}(q)$ for ^{127}I, the ordering is $S_{01}>S_{00}>S_{11}$ for each force. (b) $S_{ij}(q)$ for ^{129}Xe, the ordering is $S_{00}>S_{11}>S_{01}$ for each interaction. (c) $S_{ij}(q)$ for ^{131}Xe, the ordering is $S_{00}>S_{11}>S_{01}$ for each interaction. (d) $S_{ij}(q)$ for ^{125}Te, the ordering is $S_{00}>S_{11}>S_{01}$ for each interaction.

to values of $y=10$. We have addressed this in two ways. In Appendix B we present fits of the structure functions S_{00}, S_{01}, and S_{11} as sixth-order polynomials in y. These fits are only good for values of $y<1$. They should *not* be used beyond this value as they give meaningless results. In order to accurately represent $S(q)$ at all relevant momentum transfers, we have had to resort to a somewhat more complicated functional form. In a harmonic oscillator basis, the matrix elements of the operators $\mathcal{T}^{\rm el5}(q)$ and $\mathcal{L}^5(q)$ are precisely represented as polynomials in y times a factor of $\exp(-y)$. [The isovector Goldberger-Trieman term in $\mathcal{L}^5(q)$ complicates this slightly.] Using this form as a guide we have fit the structure functions as eighth-order polynomials in y times a factor or $\exp(-2y)$. This form has proven adequate to accurately describe the structure functions for ^{127}I and ^{131}Xe. A slightly more complicated form with a term added to mimic the effect of the Goldberger-Trieman term was required for ^{129}Xe and ^{125}Te. As an example, we present the fit for the term $S_{00}(q)$ for the Bonn A calculation of ^{127}I:

$$S_{00}(y)=e^{-2y}(0.098\,339\,3-0.489\,096y+1.1402y^2 -1.471\,68y^3+1.1717y^4-0.564\,574y^5 +0.158\,287y^6-0.023\,8874y^7+0.00\,1542\,52y^8). \tag{11}$$

We relegate the remaining formulas to Appendix C. The various fits can be acquired in a form suitable for inclusion in a Fortran program by contacting one of the authors.

In Figs. 2(a)–2(d), we present the functions $S_{ij}(y)$ for the nuclei ^{127}I, ^{129}Xe, ^{131}Xe, and ^{125}Te. The solid lines are for the calculations using the Bonn A Hamiltonian and the dashed lines are for the Nijmegen II based Hamiltonian. In order to make comparisons with other work easier, we restrict the results to values of $y\leqslant 2$ ($q^2\leqslant\sim 60\,000$ MeV^2). For illustration, in Fig. 3 we show the full structure function of ^{127}I out to $y=10$. In Figs. 4(a)–4(d), we show the full structure functions for a pure $\widetilde{B}$ ($Z_1=1$, $Z_2=Z_3=Z_4=0$) for each of the nuclei out to a value of $y=2$. In these figures each function has been normalized to the value $S(y=0)=1$ in order to highlight the similarities and differences in the shapes of the structure functions. In our definition of the $\widetilde{B}$ we use the older, EMC, values of the spin content of the proton. This convention makes it easier to compare our work to previous work on ^{131}Xe [20,44]. The precise values of a_p and a_n (or a_0 and a_1) can be found in [22]; the ratio is $a_0/a_1=0.297$.

In Figs. 4 and 5 all of the structure functions have been normalized to $S(y=0)=1$ to highlight their similarities and differences. In order to correctly gauge the true differences between the various $S(q)$, the different normalizations must be taken into account. This is easily done by using Eq. (9) and Table II. As an example, consider ^{127}I in Fig. 4(a) and in Fig. 5(a). To truly compare the structure functions each of the lines needs to be multiplied by a factor such that the ratio at $y=0$ is given by Bonn A (Woods-Saxon): Nijmegen II

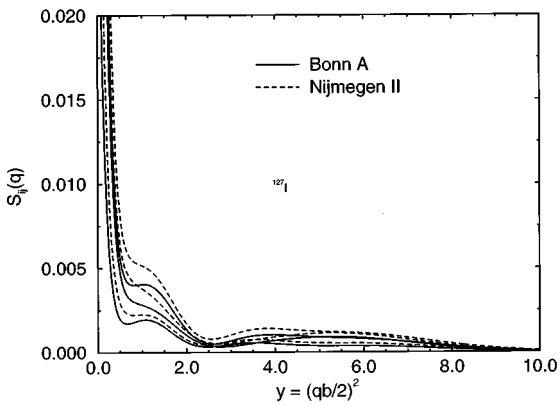

FIG. 3. Another view of (a) in Fig. 2. Here we have extended $S_{ij}(q)$ out to $y=10$ and chopped off much of the initial fall off from $S_{ij}(0)$ in order to highlight the similarities and differences between the two sets of structure functions.

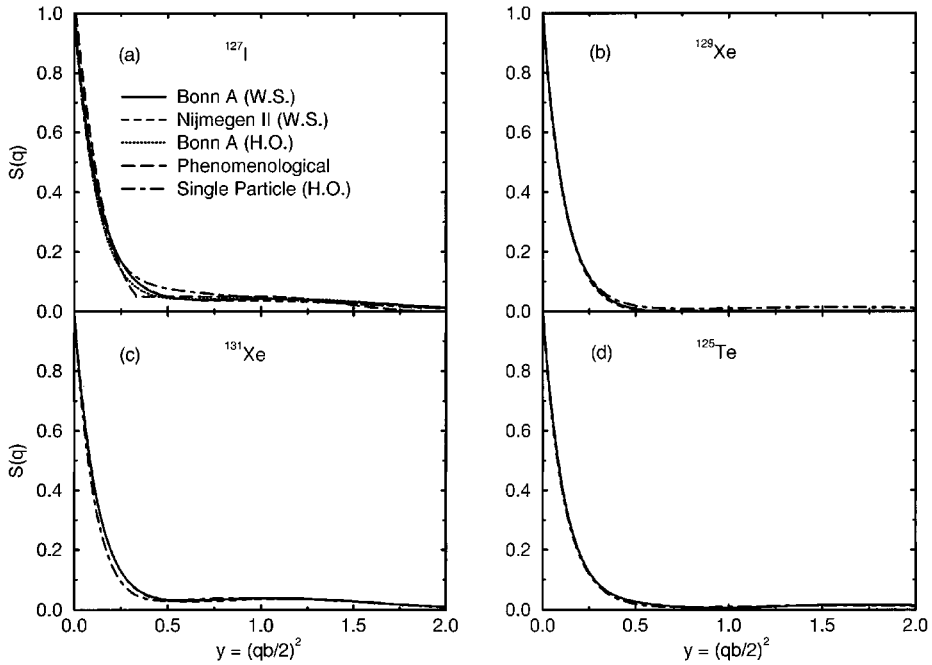

FIG. 4. The spin structure function $S(q)$ for a pure $\widetilde{B}$ $(a_0/a_1=0.297)$ for the four nuclei considered. Woods-Saxon (WS) wave functions have been used. The results using both effective interactions are plotted. Additionally, the pure single-particle estimate of $S(q)$ with harmonic oscillator (HO) wave functions is included for comparison. All structure functions have been normalized to $S(0)=1$ in order to better compare their intrinsic shapes. To truly compare the differences the functions need to be normalized using Eq. (9) and the values in Table II. (a) $S(q)$ for ^{127}I. Also included for comparison is the $S(q)$ used in [13] and the results for the Bonn A interaction using HO wave functions. (b) $S(q)$ for ^{129}Xe. (c) $S(q)$ for ^{131}Xe. (d) $S(q)$ for ^{125}Te.

(Woods-Saxon): Bonn A (harmonic oscillator): phenomenological (w/ OGM): single particle (harmonic oscillator) = 1 : 1.42 : 1 : 1/14.7 : 3.47. Similar results can be recovered for the other nuclei considered.

The line labeled phenomenological above and in the figures requires some explanation. This is a shape for a general structure function postulated and used in Ref. [13]. It is apparent from the figures that this approximation does a reasonable job in reproducing $S(q)$ for $y\leqslant 2$. It is clearly inadequate for larger values of the momentum transfer. Below $y=2$, its shortcomings are also clear but any result derived using this parametrization of $S(q)$ for ^{127}I should not be far off. The overall ^{127}I axial result of Ref. [13] is another matter, as that paper normalizes to the OGM at $y=0$. As we have shown, that model severely underestimates $S(0)$.

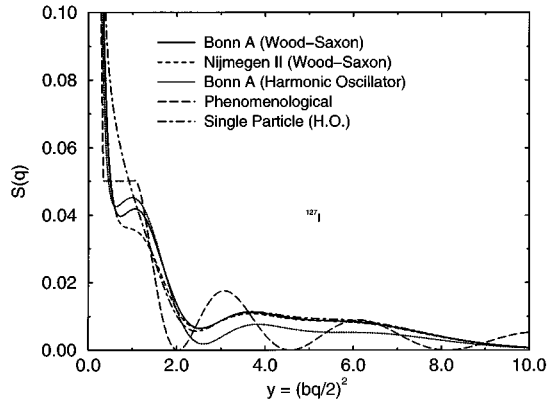

FIG. 5. Another view of (a) in Fig. 4. Here we have extended $S(q)$ out to $y=10$ and chopped off much of the initial fall off from $S(0)$ in order to highlight the similarities and differences between the various structure functions.

While the parametrization of $S(q)$ in [13] is adequate for ^{127}I (although we now advocate the use of the ^{127}I structure functions presented in the appendices), it is not applicable for all nuclei. The flattening observed in $S(q)$ near $y=1$ is the result of higher order multipoles becoming important in Eq. (8). For ^{127}I the $L=1,3,5$ multipoles all contribute to $S(q)$. For small $y(\ll 1)$, the structure function is dominated by the $L=1$ multipole. For $y\geqslant 1$, all three multipoles contribute and the higher order multipoles dominate. For $J=\frac{1}{2}$ nuclei, such as ^{129}Xe and ^{125}Te, only the $L=1$ multipole can contribute. Figures 2(b) and 2(d) and 4(b) and 4(d) clearly show that there is no flattening of $S(q)$. Hence, an approximate form like that in [13] is clearly inappropriate in these cases. In Fig. 6 we show the Bonn A derived structure functions for a pure $\widetilde{B}$ for all four nuclei. It is obvious that they cannot all be fit by a single, simple, parametrization. Figures 4 and 5 do show that the pure single-particle form factor also does an acceptable, but not compelling, job of representing the structure functions at all momentum transfers if *correctly normalized* at $y=0$. The correct single-particle form factor can be easily found by using the tables in the paper by Donnelly and Haxton of Ref. [40].

Examining the structure functions for ^{125}Te and ^{129}Xe in Fig. 6 illustrates an interesting feature. Both of these nuclei are $J=\frac{1}{2}$ nuclei with an unpaired neutron. In the ISPSM both of these nuclei would be represented by a neutron in the $3s_{1/2}$ orbital and have virtually identical properties. Table II shows that the magnetic moments are quite similar but that the distribution of the angular momentum in each nucleus is

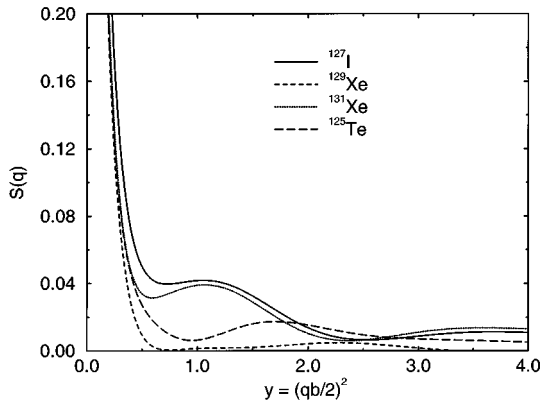

FIG. 6. The Bonn A calculations of $S(q)$ for a pure $\widetilde{B}$ for all four nuclei compared. Note the very large differences near $y=1$ between the nuclei with $J=\frac{1}{2}$ (^{129}Xe and ^{125}Te) and those with larger J.

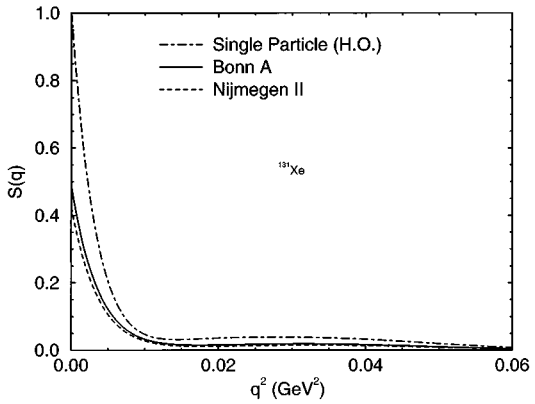

FIG. 7. The ^{131}Xe structure function for a pure $\widetilde{B}$. The single-particle structure function has been normalized to $S(0)=1$. The Bonn A and Nijmegen II calculations have been correctly normalized relative to the single-particle model. This figure is a direct analog of, and should be compared to, Fig. 2 of Ref. [20] and Fig. 3 of Ref. [44]. The major differences between these calculations and those of [20], [44] are that we find $S(0)\simeq 0.4$–0.5 vs their values of $S(0)\simeq 0.25$ and both of the other model's structure functions asymptote to the single-particle model for $q^2>0.02$ GeV^2 while these calculations stay well below the single-particle model.

quite different. This is most obvious in the orbital angular momentum $\mathbf{L}_i$ where the two distributions are quite different. Figure 6 reveals that while the structure functions have definite similarities, there are significant differences as well. We point all of this out to highlight the fact that seemingly very similar nuclei can have very different properties when examined in detail. If precise information on the spin distribution of a nucleus is required, detailed calculations must be performed.

It is also useful to consider differences in $S(q)$ that are the result of different nuclear models. $S(q)$ has been calculated for ^{131}Xe in the context of two other nuclear models, the QTDA [20] and the TFFS [44], as well as here. In Fig. 7 we show $S(q)$ for a pure $\widetilde{B}$ as a function of q^2 for ^{131}Xe. This figure is meant to be a direct analog of Fig. 2 in Ref. [20] and Fig. 3 of Ref. [44]. Examining the three figures yields some interesting conclusions. All three calculations show significant quenching compared to the single-particle estimate. The spin distribution between the QTDA and TFFS is somewhat different while the full structure functions are quite similar. While the values for $\mathbf{S}_n$ differ very little between our work and the QTDA, the difference in the values of $S(0)$ is almost a factor of 2 between the two calculations. Finally, it should be noted that both the QTDA and TFFS calculations of $S(q)$ asymptote to the single-particle structure function. This is not the case in our calculations, which are well below the single-particle estimate for all values of q^2. This can also be seen in Ref. [34] where our values of $S_{ij}(q)$ for the Bonn A calculation are compared to those of the QTDA calculation. In that comparison, it is apparent that the shell model derived structure functions have a much steeper fall off as a function of q^2.

Finally, we mention the difference between the structure functions derived using Woods-Saxon wave functions vs those derived using a harmonic oscillator basis. In Fig. 4 panel (a) and Fig. 5 we show the structure functions for ^{127}I using both sets of basis states. Significant differences between the two sets are apparent for extremely high momentum transfers but in the range that is most relevant for dark matter detection there is little difference.

In this section we have discussed the formalism of, and presented our results for, the $\widetilde{\chi}N$ axial structure function for several nuclei involved in dark matter detectors. Accurate fits which are suitable for use in calculating event rates in detectors are presented in the appendices. Several interesting features of the functions have been noted and it is apparent that no single simple parameterization of $S(q)$ is suitable for all nuclei. Finally we have compared our results to other calculations of ^{131}Xe structure functions and noted several similarities and differences that arise from different nuclear models.

IV. DISCUSSION

In this paper we have calculated the full axial response for several heavy nuclei used in a number of direct dark matter detection experiments. With this set of structure functions, there now exists accurate calculations of the axial $\widetilde{\chi}N$ response to most, if not all, nuclei used as targets in dark matter detectors. We have used the largest model spaces practical in conjunction with realistic nuclear Hamiltonians to construct our wave functions. Two different nuclear Hamiltonians have been used in order to investigate the sensitivity of our results to this particular input.

The differences in the response due to the two forces is clearly visible in Table II and Figs. 2–6. In all cases, reasonable agreement between calculation and experiment for the magnetic moment (using free particle g factors) is achieved. It is obvious from the table that the differences between the two calculations are nontrivial but that they are quite a bit smaller than the differences coming from the use of alternate nuclear models. This shows that the interaction is not the primary uncertainty in calculations of the $\widetilde{\chi}N$ nuclear response.

We have also attempted to examine the uncertainty due to the nuclear model chosen. A number of calculations of ^{131}Xe's response have been performed. We find that our calculations are in reasonable agreement with other studies of

TABLE IV. The decomposition of the angular momentum for ^{23}Na along with the calculated and experimental magnetic moments.

	$\langle \mathbf{S}_p \rangle$	$\langle \mathbf{S}_n \rangle$	$\langle \mathbf{L}_p \rangle$	$\langle \mathbf{L}_n \rangle$	μ
^{23}Na					
Experiment					2.218
Calculation	0.2477	0.0198	0.9117	0.3206	2.2196
OGM	0.1566	0.0	1.3434	0.0	N/A

the spin distribution and finite momentum response but distinct differences do exist. In the case of ^{131}Xe it is not immediately obvious which calculation is to be preferred. The calculations presented here contain more excitations within the model space and use more modern and realistic nuclear interactions than the others in the literature. By restricting excitations within this model space, the calculations presented in [20] included excitations out of the space that we worked within. Both calculations reproduce the magnetic moment well, with the QTDA calculation doing slightly better. (We note that the QTDA model, and a refined version of it, have been applied to ^{127}I and was unable to reproduce the magnetic moment with sufficient accuracy [45].) Much of the existent literature on xenon detectors uses the QTDA structure functions for ^{131}Xe. Given that the ^{131}Xe calculations presented here do not reproduce the observables with greater accuracy than those of [20], we recommend that future analyses continue to use the QTDA structure functions for ^{131}Xe. Our calculations can be used as a measure of the uncertainties introduced by nuclear models. This prescription will allow newer work to be more easily compared to earlier studies.

Another improvement incorporated into these calculations of $S(q)$ is the use of Woods-Saxon wave functions to evaluate the multipole operators in Eq. (8). The Woods-Saxon wave functions made a significant difference at extremely high momentum transfers when compared to the usual harmonic oscillator wave functions. At the more modest momentum transfers typical of ''average'' neutralinos, the difference is found to be small.

Now that these structure functions for ^{127}I, ^{129}Xe, and ^{125}Te are available, we hope that they will be used by all experiments based upon these materials. This will facilitate comparisons between different groups. To date, each experiment has used different structure functions in their analyses. A first step in this direction has already been taken by one group. The most recent analysis of the experiments based in the Gran Sasso laboratory uses the ^{127}I and ^{129}Xe structure functions presented here [11]. We hope that other groups will follow suit so that all future results can be compared on equal footing.

ACKNOWLEDGMENTS

We acknowledge useful discussions with Petr Vogel and Dao-Chen Zheng. M.T.R. gratefully acknowledges support from the Weingart Foundation and the U.S. National Science Foundation under Grant Nos. PHY94-12818 and PHY94-20470. Oak Ridge National Laboratory is managed by Lockheed Martin Energy Research Corp. for the U.S. Department of Energy under Contract No. DE-AC05-96OR22464.

APPENDIX A: ^{23}Na

All of the current dark matter detectors which use iodine as a target also use sodium. The detectors are large sodium iodide (NaI) crystals [14]. Since a detailed calculation of the axial response of ^{23}Na has not appeared in the literature, we present one here. The nucleus ^{23}Na lies in the middle of the sd shell and therefore is amenable to the same methods applied to other sd-shell nuclei. For our calculation we perform the exactly analogous calculation to those done for ^{29}Si in Ref. [22] and ^{27}Al in [23]; including the use of harmonic oscillator wave functions. The details of the calculation can be found in the above references.

For ^{23}Na we use an oscillator parameter of $b=1.6864$ fm$=(1/117.01)$ MeV^{-1}. For our adopted maximum halo velocity of $v=700$ km/sec we have $y_{\max}=0.1875$. A breakdown of the angular momentum along with a comparison of the measured and calculated magnetic moments is presented in Table IV; agreement is excellent. Table IV also shows a significant difference in $\mathbf{S}_p$ from that predicted in the OGM. Finally, in the following equations we present fits to the structure functions $S_{ij}(q)$ as third-order polynomials in y which are highly accurate to values well past $y_{\max}$.

$$S_{00}(y)=0.037\,993\,5-0.174\,341y+0.378\,299y^2-0.342\,962y^3, \tag{A1}$$

$$S_{01}(y)=0.064\,652\,5-0.350\,289y+0.910\,031y^2-0.985\,833y^3, \tag{A2}$$

TABLE V. ^{127}I.

	Bonn A			Nijmegen II		
	S_{00}	S_{01}	S_{11}	S_{00}	S_{01}	S_{11}
1	0.0982724	0.119851	0.0365375	0.116548	0.161931	0.0562404
y	−0.675013	−0.843567	−0.262676	−0.792274	−1.14026	−0.408512
y^2	2.13531	2.73535	0.875115	2.49846	3.71441	1.37775
y^3	−3.7595	−4.93029	−1.61455	−4.38312	−6.71583	−2.57019
y^4	3.77735	5.05806	1.69076	4.38495	6.89384	2.70866
y^5	−2.0091	−2.73609	−0.930164	−2.32223	−3.72586	−1.4945
y^6	0.435566	0.60084	0.206944	0.501504	0.817068	0.332885

TABLE VI. ^{129}Xe.

	Bonn A			Nijmegen II		
	S_{00}	S_{01}	S_{11}	S_{00}	S_{01}	S_{11}
1	0.0712796	−0.121583	0.0518388	0.0464592	−0.0853234	0.0391694
y	−0.480418	0.874546	−0.394855	−0.313776	0.614961	−0.299123
y^2	1.47263	−2.83165	1.34334	0.965631	−1.98471	1.00873
y^3	−2.53226	5.09221	−2.51522	−1.6666	3.54959	−1.86483
y^4	2.49681	−5.19757	2.64796	1.64774	−3.60225	1.93996
y^5	−1.30712	2.79235	−1.4557	−0.864196	1.92573	−1.05644
y^6	0.279589	−0.60881	0.322793	0.185069	−0.418234	0.232626

TABLE VII. ^{131}Xe.

	Bonn A			Nijmegen II		
	S_{00}	S_{01}	S_{11}	S_{00}	S_{01}	S_{11}
1	0.0295866	−0.0544505	0.0250499	0.0277038	−0.0497326	0.0223178
y	−0.185155	0.36762	−0.181162	−0.175382	0.338942	−0.162659
y^2	0.593387	−1.18133	0.593168	0.560377	−1.10015	0.542687
y^3	−1.03518	2.05291	−1.03886	−0.996936	1.97087	−0.98921
y^4	1.00492	−1.98269	1.00706	1.01	−1.99963	1.01495
y^5	−0.507773	0.996715	−0.50709	−0.540224	1.06809	−0.54588
y^6	0.103658	−0.202596	0.103134	0.11739	−0.231591	0.118858

TABLE VIII. ^{125}Te.

	Bonn A			Nijmegen II		
	S_{00}	S_{01}	S_{11}	S_{00}	S_{01}	S_{11}
1	0.0396831	−0.0788638	0.0391772	0.049567	−0.0993273	0.0497519
y	−0.271174	0.572717	−0.30043	−0.342464	0.731525	−0.387508
y^2	0.869383	−1.90069	1.03775	1.06657	−2.39301	1.32901
y^3	−1.56951	3.46977	−1.94604	−1.85469	4.32285	−2.49519
y^4	1.61835	−3.5546	2.02635	1.84644	−4.42823	2.6334
y^5	−0.879731	1.90199	−1.09438	−0.976196	2.39046	−1.45353
y^6	0.194048	−0.411614	0.238043	0.210989	−0.524466	0.32414

TABLE IX. ^{127}I.

	Bonn A			Nijmegen II		
$\times(e^{-2y})$	S_{00}	S_{01}	S_{11}	S_{00}	S_{01}	S_{11}
1	0.0983393	0.11994	0.0365709	0.11663	0.162054	0.056287
y	−0.489096	−0.618424	−0.194994	−0.572149	−0.836288	−0.303825
y^2	1.1402	1.50893	0.504876	1.33797	2.05944	0.794783
y^3	−1.47168	−2.07367	−0.747451	−1.72517	−2.83193	−1.17027
y^4	1.1717	1.77307	0.704344	1.37742	2.39726	1.06373
y^5	−0.564574	−0.903597	−0.393018	−0.669986	−1.21214	−0.571342
y^6	0.158287	0.26002	0.121881	0.190522	0.348612	0.172197
y^7	−0.0238874	−0.0387025	−0.0191881	−0.0291803	−0.0521813	−0.0266165
y^8	0.00154252	0.00235675	0.00121021	0.0019081	0.00320731	0.00166238
$\frac{1}{1+y}$	0.0	0.0	0.0	0.0	0.0	0.0

TABLE X. ^{129}Xe.

	Bonn A			Nijmegen II		
$\times(e^{-2y})$	S_{00}	S_{01}	S_{11}	S_{00}	S_{01}	S_{11}
1	0.0713238	−0.12166	−2.05825	0.046489	−0.0853786	−1.28214
y	−0.344779	0.644351	1.80756	−0.225507	0.453434	1.09276
y^2	0.755895	−1.52732	−1.27746	0.499045	−1.06546	−0.712949
y^3	−0.933448	2.02061	0.654589	−0.622439	1.3867	0.314894
y^4	0.690061	−1.57689	−0.221971	0.46361	−1.0594	−0.0835104
y^5	−0.302476	0.723976	0.0454635	−0.20375	0.47576	0.0105933
y^6	0.0765282	−0.190399	−0.00425694	0.0510851	−0.122077	0.000233709
y^7	−0.0103169	0.0263823	−0.000136779	−0.00670516	0.0164292	−0.000243292
y^8	0.000573919	−0.00148593	0.00004396	0.00035659	−0.000894498	0.0000221666
$\frac{1}{1+y}$	0.0	0.0	2.11016	0.0	0.0	1.32136

TABLE XI. ^{131}Xe.

	Bonn A			Nijmegen II		
$\times(e^{-2y})$	S_{00}	S_{01}	S_{11}	S_{00}	S_{01}	S_{11}
1	0.0296421	−0.0545474	0.0250994	0.0277344	−0.0497844	0.0223447
y	−0.133427	0.271757	−0.137716	−0.124487	0.247247	−0.122063
y^2	0.377987	−0.723023	0.366609	0.328287	−0.632306	0.319493
y^3	−0.579614	1.0545	−0.53851	−0.481399	0.896416	−0.466949
y^4	0.578896	−0.971333	0.492545	0.475646	−0.816445	0.428767
y^5	−0.345562	0.538422	−0.269903	−0.285177	0.452352	−0.236789
y^6	0.115952	−0.168988	0.0836943	0.0968193	−0.142686	0.0740837
y^7	−0.0201178	0.027416	−0.0133959	−0.0170957	0.0233463	−0.0119668
y^8	0.00141793	−0.00180527	0.000868668	0.00123738	−0.00156293	0.000787042
$\frac{1}{1+y}$	0.0	0.0	0.0	0.0	0.0	0.0

TABLE XII. ^{125}Te.

	Bonn A			Nijmegen II		
$\times(e^{-2y})$	S_{00}	S_{01}	S_{11}	S_{00}	S_{01}	S_{11}
1	0.0397091	−0.0789431	0.0392236	0.0495946	−0.0993873	−1.92941
y	−0.196101	0.42738	−0.229376	−0.247766	0.54303	1.68075
y^2	0.472653	−1.09331	0.622146	0.547656	−1.28816	−1.16336
y^3	−0.650229	1.55324	−0.922531	−0.665532	1.67206	0.586501
y^4	0.541926	−1.28933	0.784648	0.474621	−1.26883	−0.207302
y^5	−0.264563	0.618441	−0.382445	−0.199442	0.56728	0.0514094
y^6	0.074891	−0.16964	0.105709	0.0481866	−0.145438	−0.00869728
y^7	−0.0114632	0.0248165	−0.0154157	−0.00616326	0.0195887	0.000870366
y^8	0.000749022	−0.00152108	0.000928651	0.000322728	−0.00106519	0.0000354095
$\frac{1}{1+y}$	0.0	0.0	0.0	0.0	0.0	1.97923

$$S_{11}(y) = 0.027\,501\,3 - 0.169\,641y + 0.507\,868y^2 - 0.617\,985y^3. \quad \text{(A3)}$$

APPENDIX B: THE ABBREVIATED STRUCTURE FUNCTIONS

The fits to $S(q)$ in this appendix are only valid for $y \leqslant 1$. The fits are presented as tables of the coefficients of sixth-order polynomials in y: $S_{ij}(q) = \Sigma_{k=0}{}^{6} C_k y^k$. The first column gives the order of y^k, then the next three columns give the corresponding values of the C_k for S_{00}, S_{01}, and S_{11} for the Bonn A calculation. The last three columns present the results for the Nijmegen II calculation in the same manner. (See Tables V–VIII.)

APPENDIX C: THE FULL STRUCTURE FUNCTIONS

The fits to $S(q)$ in this appendix are good for all values of $y \leqslant 10$. The fits are presented as tables of the coefficients of eighth-order polynomials in y plus a term included to mimic the Goldberger-Trieman term present in the longitudinal multipole [20], all multiplied by a factor of $\exp(-2y)$: $S_{ij}(q) = \{\Sigma_{k=0}{}^{8} C_k y^k + C_9[1/(1+y)]\} e^{-2y}$. (See Tables IX–XII.) The first column gives the order of y^k, then the next three columns give the corresponding values of the C_k for S_{00}, S_{01}, and S_{11} for the Bonn A calculation. The last 3 columns present the results for the Nijmegen II calculation in the same manner. An example of the table's use can be found by comparing Eq. (11) to the entries for S_{00} in the Bonn A portion of the Table IX.

[1] G. Jungman, M. Kamionkowski, and K. Griest, Phys. Rep. **267**, 195 (1996).
[2] M. S. Turner, Phys. Scr. **T36**, 167 (1991); J. Ellis, *ibid.* **T36**, 142 (1991).
[3] C. Alcock *et al.*, preprint, submitted to Astrophys. J.
[4] E. I. Gates, G. Gyuk, and M. S. Turner, Phys. Rev. D **53**, 4138 (1996).
[5] C. J. Copi, D. N. Schramm, and M. S. Turner, Phys. Rev. Lett. **75**, 3981 (1995); L. M. Krauss, in *Proceedings of the International Workshop on the Identification of Dark Matter*, edited by N. Spooner (World Scientific, Singapore, to be published).
[6] H. E. Haber and G. L. Kane, Phys. Rep. **117**, 75 (1985).
[7] J. Ellis, J. S. Hagelin, D. V. Nanopoulos, K. A. Olive, and M. Srednicki, Nucl. Phys. **B238**, 453 (1984).
[8] M. Kamionkowski, Phys. Rev. D **44**, 3021 (1991).
[9] K. Fushimi *et al.*, Phys. Rev. C **47**, R425 (1993); H. Ejiri, K. Fushimi, and H. Ohsumi, Phys. Lett. B **317**, 14 (1993).
[10] M. W. Goodman and E. Witten, Phys. Rev. D **31**, 3059 (1985).
[11] A. Bottino *et al.*, Report No. hep-ph/9612451, 1996.
[12] A. Bottino *et al.*, Phys. Lett. B **295**, 330 (1992).
[13] P. F. Smith *et al.*, Phys. Lett. B **379**, 299 (1996).
[14] R. Bernabei, Riv. Nuovo Cimento **18**, 1 (1995).
[15] D. B. Cline, Nucl. Phys. B, Proc. Suppl. **51**, 163 (1996).
[16] V. A. Bednyakov, H. V. Klapdor-Kleingrothaus, and S. G. Kovalenko, Phys. Rev. D **50**, 7128 (1994).
[17] P. L. Anthony *et al.*, Phys. Rev. D **54**, 6620 (1996).
[18] G. L. Kane and J. D. Wells, Phys. Rev. Lett. **76**, 4458 (1996); S. Ambrosanio *et al.*, Phys. Rev. D **55**, 1372 (1997).
[19] J. Engel, S. Pittel, and P. Vogel, Int. J. Mod. Phys. E **1**, 1 (1992).
[20] J. Engel, Phys. Lett. B **264**, 114 (1991).
[21] B. A. Brown and B. H. Wildenthal, Annu. Rev. Nucl. Part. Sci. **38**, 29 (1988).
[22] M. T. Ressell *et al.*, Phys. Rev. D **48**, 5519 (1993).
[23] J. Engel, M. T. Ressell, I. S. Towner, and W. E. Ormand, Phys. Rev. C **52**, 2216 (1995).
[24] A. F. Pacheco and D. Strottman, Phys. Rev. D **40**, 2131 (1989).
[25] J. Engel, S. Pittel, W. E. Ormand, and P. Vogel, Phys. Lett. B **275**, 119 (1992).
[26] M. Hjorth-Jensen, T. T. S. Kuo, and E. Osnes, Phys. Rep. **264**, 126 (1996).
[27] V. G. J. Stoks *et al.*, Phys. Rev. C **49**, 2950 (1994).
[28] E. Caurier, code ANTOINE, Strasbourg, 1989.
[29] B. R. Barrett, R. G. L. Hewitt, and R. J. McCarthy, Phys. Rev. C **3**, 1137 (1971); D. C. Zheng, B. R. Barrett, J. P. Vary, W. C. Haxton, and C.-L. Song, *ibid.* **52**, 2488 (1995).
[30] J. Engel and P. Vogel, Phys. Rev. D **40**, 3132 (1989).
[31] F. Iachello, L. M. Krauss, and G. Maino, Phys. Lett. B **254**, 220 (1991).
[32] J. Ellis and R. A. Flores, Nucl. Phys. **B307**, 883 (1988); A. K. Drukier, K. Freese, and D. N. Spergel, Phys. Rev. D **33**, 3495 (1986).
[33] M. A. Nikolaev and H. V. Klapdor-Kleingrothaus, Z. Phys. A **345**, 373 (1993).
[34] J. Engel, in *Proceedings of the International Workshop on the Identification of Dark Matter* [5].
[35] B. A. Brown and B. H. Wildenthal, Nucl. Phys. **A474**, 290 (1987).
[36] W. A. Richter *et al.*, Nucl. Phys. **A523**, 325 (1991).
[37] K. Griest and L. Roskowski, Phys. Rev. D **46**, 3309 (1992).
[38] K. Griest, M. Kamionkowski, and M. S. Turner, Phys. Rev. D **41**, 3565 (1990).
[39] K. A. Olive and M. Srednicki, Nucl. Phys. **B355**, 208 (1991).
[40] J. D. Walecka, in *Muon Physics*, edited by V. W. Hughes and C. S. Wu (Academic Press, New York, 1975), Vol. 2, p. 113; T. W. Donnelly and R. D. Peccei, Phys. Rep. **50**, 1 (1979); T. W. Donnelly and W. C. Haxton, At. Data Nucl. Data Tables **23**, 103 (1979).
[41] G. F. Bertsch, *The Practitioner's Shell Model* (North-Holland, Amsterdam, 1972), p. 1.
[42] H. P. Blok and J. H. Heisenberg, in *Computational Nuclear Physics 1*, edited by K. Langanke, J. A. Maruhn, and S. E. Koonin (Springer-Verlag, Berlin, 1991), p. 190.
[43] E. K. Warburton, J. A. Becker, and B. A. Brown, Phys. Rev. C **41**, 1147 (1990).
[44] M. A. Nikolaev and H. V. Klapdor-Kleingrothaus, Z. Phys. A **345**, 183 (1993).
[45] J. Engel, S. Pittel, and P. Vogel, Phys. Rev. C **50**, 1702 (1994).